

2 **Improved Neutrino-Induced-Muon Momentum**  
3 **Determination by Multiple Coulomb Scattering in the**  
4 **MicroBooNE LArTPC from Tuning the Highland**  
5 **Formula**

---

6 **The MicroBooNE Collaboration**

7 **ABSTRACT:** Liquid argon time projection chambers (LArTPCs) are an important detector technology for neutrino physics. This technology provides precise three-dimensional reconstruction of charged particle tracks that traverse the detector medium. We discuss a technique for measuring a charged particle's momentum by means of multiple Coulomb scattering (MCS) in the MicroBooNE LArTPC, which does not require the full particle ionization track to be contained inside of the detector volume as other track momentum reconstruction methods do (range-based momentum reconstruction and calorimetric momentum reconstruction). We motivate use of this technique, prescribe a tuning of the underlying theory formula, quantify its performance on fully contained beam-neutrino-induced muon tracks both in simulation and in data, and quantify its performance on exiting muon tracks in simulation. We find agreement between data and simulation for contained tracks, with a small bias in the momentum reconstruction and with resolutions that vary as a function of track length, decreasing from about 10% for the shortest (one meter long) tracks to 5% for longer (several meter) tracks. For exiting muons with at least one meter of track contained, we find a similarly small bias, and a resolution which is better than 15% for muons with momentum below 2 GeV/c though worse at higher momenta due to detector resolution effects.

---

|    |                                                                            |    |
|----|----------------------------------------------------------------------------|----|
| 22 | <b>Contents</b>                                                            |    |
| 23 | <b>1 Introduction and Motivation</b>                                       | 1  |
| 24 | <b>2 Multiple Coulomb Scattering (MCS)</b>                                 | 2  |
| 25 | 2.1 Tuning the Highland Formula for Argon                                  | 3  |
| 26 | <b>3 MCS Implementation Using the Maximum Likelihood Method</b>            | 5  |
| 27 | 3.1 Track Segmentation and Scattering Angle Computation                    | 6  |
| 28 | 3.2 Maximum Likelihood Theory                                              | 6  |
| 29 | 3.3 Maximum Likelihood Implementation                                      | 7  |
| 30 | <b>4 Range-based Energy Validation from Simulation</b>                     | 7  |
| 31 | <b>5 MCS Performance on Beam Neutrino-Induced Muons in MicroBooNE Data</b> | 9  |
| 32 | 5.1 Input Sample                                                           | 9  |
| 33 | 5.2 Event Selection                                                        | 9  |
| 34 | 5.3 Highland Validation                                                    | 10 |
| 35 | 5.4 MCS Momentum Validation                                                | 10 |
| 36 | 5.5 Impact of Highland Formula Tuning                                      | 11 |
| 37 | <b>6 MCS Performance on Existing Muons in MicroBooNE Simulation</b>        | 11 |
| 38 | <b>7 Conclusions</b>                                                       | 13 |

---

## 39 **1 Introduction and Motivation**

40 MicroBooNE (Micro Booster Neutrino Experiment) is an R&D experiment that uses a large Liquid  
41 Argon Time Projection Chamber (LArTPC) to investigate the excess of low energy events observed  
42 by the MiniBooNE experiment [1] and to study neutrino-argon cross-sections. MicroBooNE is part  
43 of the Short-Baseline Neutrino (SBN) [2] physics program at the Fermi National Accelerator Lab-  
44 oratory (Fermilab) along with two other LArTPCs: the Short Baseline Near Detector (SBND) and  
45 the Imaging Cosmic And Rare Underground Signal (ICARUS) detector. MicroBooNE also per-  
46 forms important research and development in terms of detector technology and event reconstruc-  
47 tion techniques for future LArTPC experiments including DUNE (Deep Underground Neutrino  
48 Experiment).

49  
50 The MicroBooNE detector [3] consists of a rectangular time projection chamber (TPC) with  
51 dimensions 2.6 m width  $\times$  2.3 m height  $\times$  10.4 m length located 470 m away from the Booster  
52 Neutrino Beam (BNB) target. LArTPCs allow for precise three-dimensional reconstruction of par-  
53 ticle interactions. The  $x$ - direction of the TPC corresponds to the drift coordinate, the  $y$ - direction

54 is the vertical direction, and the  $z$ - direction is the direction along the beam. The mass of active  
55 liquid argon in the MicroBooNE TPC is 89 tons, with the total cryostat containing 170 tons of  
56 liquid argon.

57  
58 A set of 32 photomultiplier tubes (PMTs) and three planes of wires with 3 mm spacing at  
59 angles of 0, and  $\pm 60$  degrees with respect to the vertical are located in the TPC for event recon-  
60 struction. The cathode plane operating voltage is -70 kV. In a neutrino interaction, a neutrino from  
61 the beam interacts with an argon nucleus and the charged outgoing secondary particles traverse the  
62 medium, losing energy and leaving an ionization trail. The resulting ionization electrons drift to the  
63 anode side of the TPC, containing the wire planes. The passage of these electrons past the first two  
64 wire planes induces a signal in them, and their collection on the third plane also generates a signal.  
65 These signals are used to create three distinct two-dimensional views (in terms of wire and time)  
66 of the event. Combining these wire signals with timing information from the PMTs allows for full  
67 three-dimensional reconstruction of the event. The fiducial volume used in this analysis is defined  
68 as the full TPC volume reduced by 20 cm from both the cathode plane and the anode wire planes,  
69 by 26.5 cm from both the top and bottom walls of the TPC, by 20 cm from the beam-entering wall  
70 of the TPC, and by 36.8 cm from the beam-exiting wall of the TPC. This fiducial volume, corre-  
71 sponding to a mass of 55 tons, was chosen to reduce the impact of electric field nonuniformities  
72 near the edges of the TPC which have been characterized in parts of the TPC where the effect is  
73 expected to be the largest, but not fully calibrated out in data [4].

74  
75 The Booster Neutrino Beam (BNB) is predominantly composed of muon neutrinos ( $\nu_\mu$ ) with  
76 a peak neutrino energy of about 0.7 GeV, some of which undergo charge-current ( $\nu_\mu$ CC) interac-  
77 tions in the TPC and produce muons. For muon tracks that are completely contained in the TPC,  
78 it is straightforward to calculate their momentum with a measurement of the length of the parti-  
79 cle's track, or with calorimetric measurements which come from wire signal size measurements.  
80 Around half of the muons from BNB  $\nu_\mu$ CC interactions in MicroBooNE are not fully contained  
81 in the TPC, and therefore using a length-based or calorimetry-based method to determine the mo-  
82 ments for these uncontained tracks is not a possibility. The only way to compute the energy of a  
83 non-contained three-dimensional track is by means of multiple Coulomb scattering (MCS).

84  
85 In this paper we summarize the theory of multiple Coulomb scattering and describe how the  
86 underlying Highland formula is retuned based on MC simulation for use specifically in liquid ar-  
87 gon. We present a maximum likelihood based algorithm that is used to determine the momentum  
88 of particles in a LArTPC and demonstrate that this technique works for a sample of fully con-  
89 tained muons from BNB  $\nu_\mu$ CC interactions, with bias and resolutions quantified. Additionally,  
90 quantification of performance on exiting tracks is presented.

## 91 2 Multiple Coulomb Scattering (MCS)

92 Multiple Coulomb scattering (MCS) occurs when a charged particle enters a medium and under-  
93 goes electromagnetic scattering with atomic nuclei. This scattering perturbs the original trajectory  
94 of the particle within the material (Figure 1). For a given initial momentum  $p$ , the angular deflection

95 scatters of a particle in either the  $x'$  direction or  $y'$  direction (as indicated in the aforementioned figure)  
 96 form a Gaussian distribution centered at zero with an RMS width,  $\sigma_o^{HL}$ , given by the Highland  
 97 formula [5]:

$$\sigma_o^{HL} = \frac{S_2}{p\beta c} z \sqrt{\frac{\ell}{X_0}} \left[ 1 + \epsilon \times \ln\left(\frac{\ell}{X_0}\right) \right] \quad (2.1)$$

98 where  $\beta$  is the ratio of the particle's velocity to the speed of light assuming the particle is a muon,  
 99  $\ell$  is the distance traveled inside the material,  $z$  is the magnitude of the charge of the particle (unity,  
 100 for the case of muons), and  $X_0$  is the radiation length of the target material (taken to be a constant  
 101 14 cm in liquid argon).  $S_2$  and  $\epsilon$  are constants defined to be 13.6 MeV and 0.0038, respectively.  
 102 In this study, a modified version of the Highland formula is used that includes a detector-inherent  
 103 angular resolution term,  $\sigma_o^{res}$

$$\sigma_o = \sqrt{(\sigma_o^{HL})^2 + (\sigma_o^{res})^2} \quad (2.2)$$

104 For this analysis, the  $\sigma_o^{res}$  term is given a fixed value of 3 mrad which has been determined to be  
 105 an acceptable value based on simulation studies of higher momenta muons. At 4.5 GeV/c muon  
 106 momentum and  $l \approx X_0$ , Equation 2.1 predicts an RMS angular scatter of 3 mrad, comparable to the  
 107 detector resolution. The fully contained muons addressed in this analysis have momenta below 1.5  
 108 GeV/c, making detector resolution negligible.

109

110 With the Highland formula, the momentum of a track-like particle can be determined using  
 111 only the 3D reconstructed track it produces in the detector, without any calorimetric or track range  
 112 information. Within neutrino physics, past emulsion detectors like the DONUT [6] and OPERA  
 113 [7] experiments have used MCS to determine particle momenta. Additionally, the MACRO [8]  
 114 experiment at Gran Sasso Laboratory utilized this technique. While the original method for using  
 115 MCS to determine particle momentum in a LArTPC used a Kalman Filter and was described by  
 116 the ICARUS collaboration [9] (more recently the ICARUS collaboration describes another method  
 117 [10]), the maximum-likelihood based method discussed in this paper for use in the MicroBooNE  
 118 detector is described in detail in Section 3.

## 119 2.1 Tuning the Highland Formula for Argon

120 The Highland formula as written in Equation 2.1 originated from a 1991 publication by G. R. Lynch  
 121 and O. I. Dahl [11]. The constants in the equation ( $S_2$  and  $\epsilon$ ) were determined using a global fit  
 122 over MCS simulated data using a modified GEANT simulation package of 14 different elements  
 123 and 7 thickness ranges. All of the simulated particles were relativistic, with  $\beta = 1$ . The materials  
 124 in which they studied scattering ranged from hydrogen (with Z=1) to uranium (with Z=92). Given  
 125 that the constants in the formula were determined from a single fit to a wide range of Z with a  
 126 wide range of material thicknesses, there is reason to believe that these constants should differ for  
 127 scattering specifically in liquid argon with  $l \approx X_0$ . There is also reason to believe that these con-  
 128 stants might be momentum-dependent for particles with  $\beta < 1$ , which is the case for some of the  
 129 contained muons in this analysis.

130

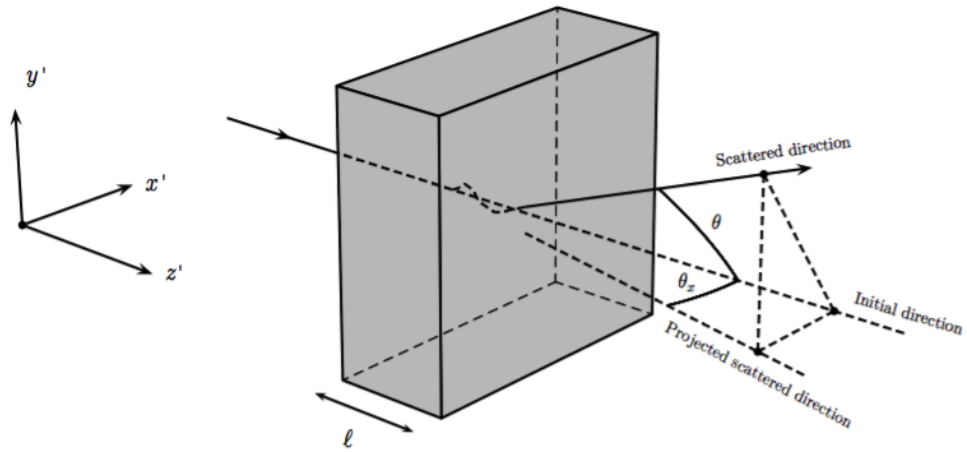


**Figure 1.** The particle's trajectory is deflected as it traverses through the material.

131 In order to re-tune these constants to liquid argon, a large sample of muons were simulated  
 132 with GEANT4 [12] in the MicroBooNE TPC and their true angular scatters were used in a fit,  
 133 with  $l = X_0$ . The reason for using  $l = X_0$  is that the Highland formula simplifies to remove its  
 134 dependence on the  $\epsilon$  constant term:

$$\sigma_o^{HL} = \frac{S_2}{p\beta c} \quad (2.3)$$

135 The  $S_2$  constant in Equation 2.3 was fit for as a function of true muon momentum at each  
 136 scatter, in order to explore the  $\beta$  dependence of this constant. The fitted constant value as a function  
 137 of true momentum is shown in Figure 2.

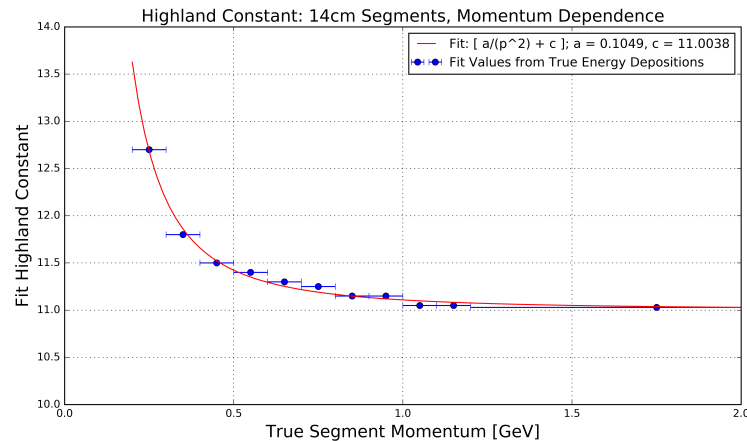


**Figure 2.** Fitted Highland constant  $S_2$  as a function of true segment momentum for  $l = X_0$  simulated muons in the MicroBooNE LArTPC. Blue x- error bars indicate the true momentum bin width with data points drawn at the center of each bin. Shown in red is a fit to these data points with functional form  $\frac{a}{p^2} + c$ , with best fit values for constants  $a$  and  $c$  shown in the legend.

138 It can be seen that the fitted value of  $S_2$  is always less than the nominal 13.6 for momentum  
 139 greater than 0.25 GeV/c and asymptotically approaches a constant at higher momentum (where  
 140  $\beta = 1$ ) of about 11.0. The value increases in the momentum region where  $\beta < 1$ . Shown in red  
 141 is a fit to these data points with functional form  $\frac{a}{p^2} + c$ , with best fit values for floating constants  $a$   
 142 and  $c$  being 0.105 and 11.004 respectively. This functional form was chosen because it fit the data  
 143 well, and asymptotically approaches a constant value when  $\beta$  approaches 1. This function, used as  
 144 a replacement for the  $S_2$  constant in the Highland formula, will henceforth be referred to as  $\kappa(p)$ :

$$\kappa(p) = \frac{0.105}{p^2} + 11.004 \quad (2.4)$$

145 To visualize the Highland formula for  $\ell = X_0$  both before and after the  $\kappa(p)$  replacement,  
 146 see Figure 3. It is recommended that future LArTPC experiments use this parameterization of the  
 147 Highland formula, or at the very least conduct their own studies to tune the Highland formula for  
 148 scattering specifically in argon. This formulation can also be checked in LAr-based test-beam ex-  
 149 periments like LArIAT [13].

150

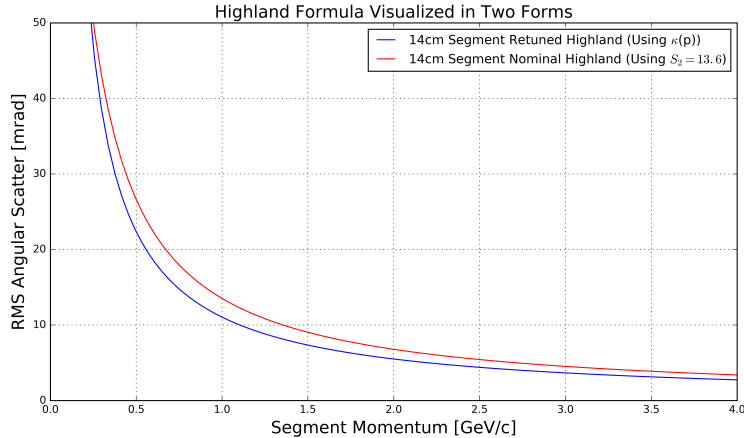


**Figure 3.** The Highland scattering RMS  $\sigma_o$  for 14 cm segment lengths and 0 detector-inherent angular resolution as a function of true momentum before and after tuning. In red is shown Equation 2.3 (the nominal Highland formula using  $S_2 = 13.6$ ) and in blue is the retuned Highland formula (replacing  $S_2$  with  $\kappa(p)$ ).

151 With  $\ell = X_0$ , the form of the Highland equation used in this analysis is therefore:

$$\sigma_o^{RMS} = \sqrt{(\sigma_o)^2 + (\sigma_o^{res})^2} = \sqrt{\left(\frac{\kappa(p)}{p\beta c}\right)^2 + (\sigma_o^{res})^2} \quad (2.5)$$

### 152 3 MCS Implementation Using the Maximum Likelihood Method

153 This section describes exactly how the phenomenon of multiple Coulomb scattering is leveraged  
 154 to determine the momentum of a muon track reconstructed in a LArTPC. In general, the approach  
 155 is as follows:

- 156 1. The three-dimensional track is divided into segments of configurable length.
- 157 2. The scattering angles between consecutive segments are measured.
- 158 3. Those angles combined with the modified, tuned Highland formula (Equation 2.5) are used  
159 to build a likelihood that the particle has a specific momentum, taking into account energy  
160 loss in upstream segments of the track.
- 161 4. The momentum corresponding to the maximum of the likelihood is chosen to be the MCS  
162 computed momentum.
- 163 Each of these steps is discussed in detail in the following subsections.

164

### 165 3.1 Track Segmentation and Scattering Angle Computation

166 Track segmentation refers to the subdivision of three-dimensional reconstructed trajectory points  
167 of a reconstructed track into portions of definite length. In this analysis, the tracks are automati-  
168 cally reconstructed by the “pandoraNuPMA” projection matching algorithm which constructs the  
169 three-dimensional trajectory points by combining two-dimensional hits reconstructed from signals  
170 on the different wire planes along with timing information from the photomultiplier tubes [14].  
171 The segmentation routine begins at the start of the track, and iterates through the trajectory points  
172 in order, defining segment start and stop points based on the straight-line distance between them.  
173 There is no overlap between segments. Given the subset of the three-dimensional trajectory points  
174 that corresponds to one segment of the track, a three-dimensional linear fit is applied to the data  
175 points, weighting all trajectory points equally in the fit. In this analysis, a segment length of 14 cm  
176 is used, which is a tunable parameter that has been chosen as described in the derivation of  $\kappa(p)$   
177 (Equation 2.4).

178

179 With the segments defined, the scattering angles between the linear fits from adjacent segments  
180 are computed. A coordinate transformation is performed such that the  $z'$  direction is oriented along  
181 the direction of the linear fit to the first of the segment pair. The  $x'$  and  $y'$  coordinates are then  
182 defined such that all of  $x'$ ,  $y'$ , and  $z'$  are mutually orthogonal and right-handed, as shown in Figure  
183 1. The scattering angles both with respect to the  $x'$  direction and the  $y'$  direction are then computed  
184 to be used by the MCS algorithm. Note that only the scattering angle with respect to the  $x'$  direction  
185 is drawn in Figure 1.

### 186 3.2 Maximum Likelihood Theory

187 The normal probability distribution for a scattering angle in either the  $x'$  or  $y'$  direction,  $\Delta\theta$  with  
188 an expected gaussian error  $\sigma_o$  and mean of zero is given by:

$$f_X(\Delta\theta) = (2\pi\sigma_o^2)^{-\frac{1}{2}} \exp\left(-\frac{1}{2}\left(\frac{\Delta\theta}{\sigma_o}\right)^2\right) \quad (3.1)$$

189 Here,  $\sigma_o$  is the RMS angular deflection computed by the modified, tuned Highland formula  
190 (Equation 2.5), which is a function of both the momentum and the length of that segment. Since

191 energy is lost between segments along the track,  $\sigma_o$  increases for each angular measurement along  
 192 the track so we replace  $\sigma_o$  with  $\sigma_{o,j}$ , where  $j$  is an index representative of the segment.

193

194 To get the likelihood, one takes the product of  $f_X(\Delta\theta_j)$  over all  $n$  of the  $\Delta\theta_j$  segment-to-  
 195 segment scatters along the track. With some manipulation, this product becomes

$$L(\sigma_{o,1}, \dots, \sigma_{o,n}; \Delta\theta_1, \dots, \Delta\theta_n) = (2\pi)^{-n} \times \prod_{j=1}^n (\sigma_{o,j})^{-1} \times \exp\left(-\frac{1}{2} \sum_{j=1}^n \left(\frac{\Delta\theta_j}{\sigma_{o,j}}\right)^2\right) \quad (3.2)$$

196 In practice, rather than maximizing the likelihood it is more computationally convenient to  
 197 instead minimize the negative log likelihood. Inverting the sign and taking the natural logarithm of  
 198 the likelihood  $L$  gives an expression that is related to a  $\chi^2$

$$-l(\mu_o; \sigma_{o,1}, \dots, \sigma_{o,n}; \Delta\theta_1, \dots, \Delta\theta_n) = -\ln(L) = \frac{n}{2} \ln(2\pi) + \sum_{j=1}^n \ln(\sigma_{o,j}) + \frac{1}{2} \sum_{j=1}^n \left(\frac{\Delta\theta_j}{\sigma_{o,j}}\right)^2 \quad (3.3)$$

### 199 3.3 Maximum Likelihood Implementation

200 Given a set of angular deflections in the  $x'$  and  $y'$  directions for each segment as described in  
 201 Section 3.1 a raster scan over the postulated initial energy,  $E_t$ , in steps of 1 MeV up to 7.5 GeV is  
 202 computed and the step with the smallest negative log likelihood (Equation 3.3) is chosen as the final  
 203 MCS energy. Note that Equation 3.3 includes a  $\sigma_{o,j}$  term which changes for consecutive segments  
 204 because their energy is decreasing. The energy of the  $j$ th segment is related to  $E_t$  by

$$E_j = E_t - E_j^{\text{upstream}} \quad (3.4)$$

205 where  $E_j^{\text{upstream}}$  is the energy loss upstream of this segment, computed by integrating the muon  
 206 stopping power curve given by the Bethe-Bloch equation described by the Particle Data Group  
 207 (PDG) [16] along the length of track upstream of this segment. Note that Equation 3.4 introduces a  
 208 minimum allowable track energy determined by the length of the track, as  $E_j$  must remain positive.  
 209 This value of segment energy is converted to a momentum,  $p$ , with the usual energy-momentum  
 210 relation assuming the muon mass, and is then used to predict the RMS angular scatter for that  
 211 segment ( $\sigma_o$ ) by way of Equation 2.5.

## 212 4 Range-based Energy Validation from Simulation

213 In order to quantify the performance of the MCS energy estimation method on fully contained  
 214 muons in data, an additional handle on energy is needed. Here, range-based energy,  $E_{\text{range}}$  is used  
 215 since when dealing with data the true energy,  $E_{\text{true}}$  will not be known. The stopping power of  
 216 muons in liquid argon is well described by the continuous-slowing-down-approximation (CSDA)  
 217 by the particle data group (PDG) with agreement to data at the sub-percent level [15] [17] [18].  
 218 By using a linear interpolation between points in the cited PDG stopping power table, the length  
 219 of a track can be used to reconstruct the muon's total energy with good accuracy. A simulated  
 220 sample of fully contained BNB neutrino-induced muons longer than one meter is used to quantify  
 221 the bias and resolution for the range-based energy estimation technique. The range is defined

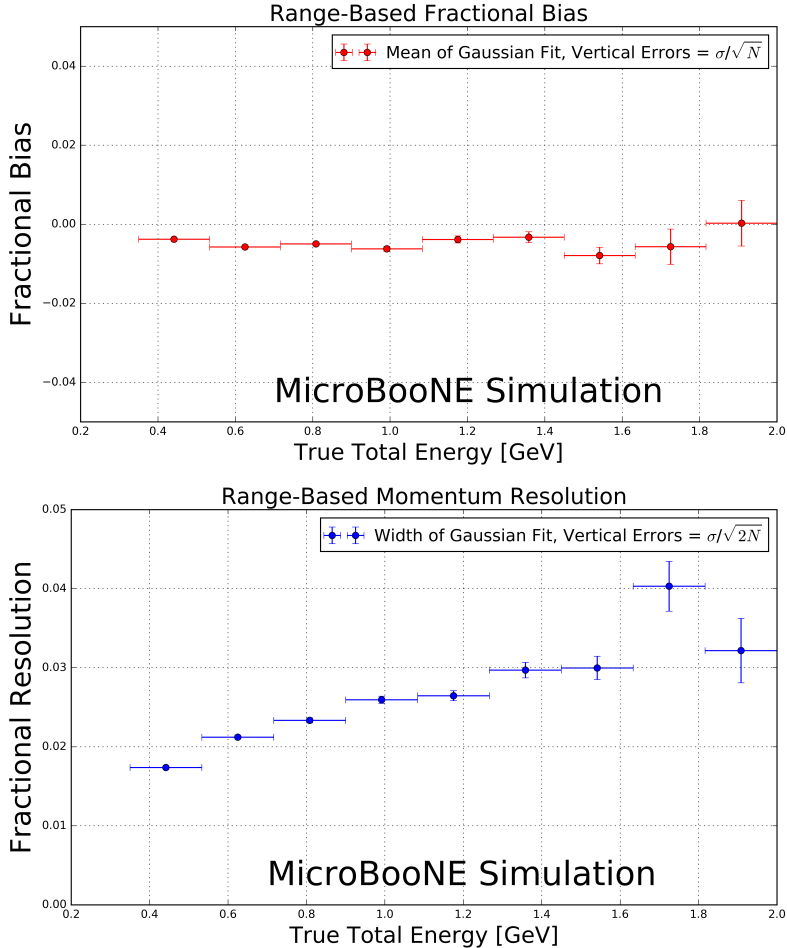


**Figure 4.** Range-based energy fractional bias (top) and resolution (bottom) from a sample of simulated fully contained BNB neutrino-induced muons using true starting and stopping positions of the track. The bias is less than 1% and the resolution is below  $\approx 4\%$ .

as the straight-line distance between the true starting point and true stopping point of a muon, even though the trajectories are not in fact perfectly straight lines. The bias and resolution are computed in bins of true total energy of the muons by fitting a gaussian to a distribution of the fractional energy difference ( $\frac{E_{Range} - E_{True}}{E_{True}}$ ) in each bin. The mean of each gaussian indicates the bias for that true energy bin, and the width indicates the resolution. Figure 4 shows the bias and resolution for the range-based energy reconstruction method. It can be seen that the bias is negligible and the resolution for this method of energy reconstruction increases slightly with true muon energy but remains on the order of 2-4%. Based on this figure, it is clear that range-based energy (and therefore range-based momentum) is a good handle on the true energy (momentum) of a reconstructed contained muon track in data, assuming that the track is well reconstructed in terms of length.

233 **5 MCS Performance on Beam Neutrino-Induced Muons in MicroBooNE Data**

234 **5.1 Input Sample**

235 The input sample to this portion of the analysis is  $\sim 5 \times 10^{19}$  protons-on-target worth of trig-  
236 gered BNB neutrino interactions in MicroBooNE data, which is a small subset (less than 10%)  
237 of the nominal amount of beam scheduled to be delivered to the detector. These events are run  
238 through a fully automated reconstruction chain which produces reconstructed objects including  
239 three-dimensional neutrino interaction points (vertices), three-dimensional tracks (as described in  
240 Section 3.1) for each outgoing secondary particle from the interaction, and PMT-reconstructed op-  
241 tical flashes from the interaction scintillation light. The fiducial volume used in this analysis is  
242 defined in Section 1.

243 **5.2 Event Selection**

244 The following selection cuts are placed on the aforementioned reconstructed objects to select  $\nu_\mu$   
245 charged-current interactions in which a candidate muon track exiting the interaction vertex is fully  
246 contained within the fiducial volume:

- 247 1. The event must have at least one bright optical flash in coincidence with the expected BNB  
248 neutrino arrival time.
- 249 2. Two or more reconstructed tracks must originate from the same reconstructed vertex within  
250 the fiducial volume.
- 251 3. The span in  $z-$  of the candidate muon track must be within 70 cm of the  $z-$  position of the  
252 optical flash as determined by the pulse height and timing of signals in the 32 PMTs.
- 253 4. For events with exactly two tracks originating from the vertex, additional calorimetric-based  
254 cuts are applied to mitigate backgrounds from cosmics in time with the passage of the beam  
255 which produce a Michel electron reconstructed as a track.
- 256 5. The longest track originating from the vertex is assumed to be a muon, and it must be fully  
257 contained within the fiducial volume.
- 258 6. The longest track must be at least one meter long, in order to have enough sampling points  
259 in the MCS likelihood to obtain a reasonable estimate of its momentum.

260 These cuts were chosen to select a sample of tracks with high purity. In this sample of Micro-  
261 BooNE data, 598 events (tracks) remain after all event selection cuts. The relatively low statistics  
262 in this sample is due to the limited input sample, described in Section 5.1. Each of these events  
263 (tracks) were scanned by hand with a 2D interactive event display showing the raw wire signals of  
264 the interaction from each wire plane, with the 2D projection of the reconstructed muon track and  
265 vertex overlaid. The scanning was done to ensure the track was well reconstructed with start point  
266 close to the reconstructed vertex and end point close to the end of the visible wire-signal track in all  
267 three planes. Additionally the scanning was to remove obvious mis-identification (MID) topologies  
268 such as cosmic rays inducing Michel electrons at the reconstructed neutrino vertex which were not  
269 successfully removed by the automated event selection cuts. After rejecting events (tracks) based  
270 on hand scanning, 396 tracks remain for analysis.

271 **5.3 Highland Validation**

272 The Highland formula indicates that histograms of the track segment-by-segment angular deviations  
 273 in both the  $x'$  and  $y'$  directions divided by the width predicted from the Highland equation  
 274  $\sigma_o^{HL}$  (Equation 2.5) should be gaussian with a width of unity. In order to calculate the momentum  
 275  $p$  in the Highland equation,  $p$  for each segment is computed with Equation 3.4 where  $E_t$  comes  
 276 from the converged MCS computed momentum of the track. For each consecutive pair of segments  
 277 in this sample of 396 tracks, the angular scatter in milliradians divided by the Highland expected  
 278 RMS in milliradians is an entry in the area-normalized histogram shown in Figure 5. From this  
 279 figure we can see that the distribution has an RMS of unity, thus validating the MCS technique  
 280 used in this analysis.

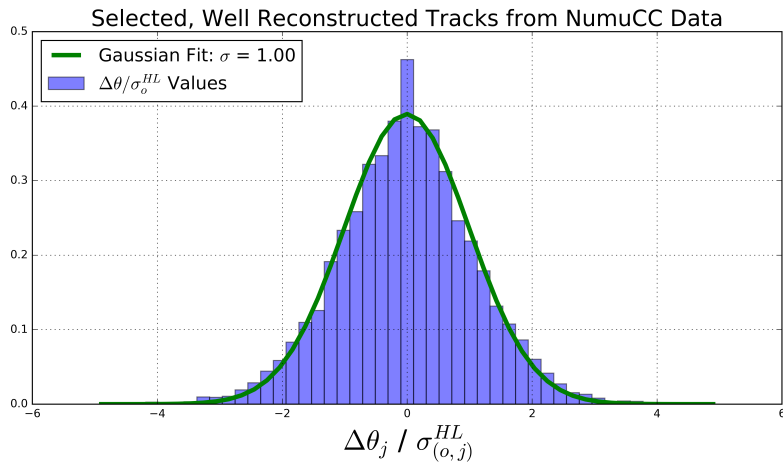


**Figure 5.** Segment-to-segment measured angular scatters in both the  $x'$  and  $y'$  directions divided by the Highland formula (Equation 2.1) predicted width  $\sigma_o^{HL}$  for the automatically selected beam neutrino-induced fully contained muon sample in MicroBooNE data after hand scanning to remove poorly reconstructed tracks and obvious mis-identification (MID) topologies. That the fitted Gaussian distribution has a width of unity indicates that the basis of the MCS technique is validated.

281 **5.4 MCS Momentum Validation**

282 The MCS momentum versus range-based momentum for this sample of 396 tracks can be seen  
 283 in Figure 6. The fractional bias and resolution as a function of range-based momentum for this  
 284 sample is shown in Figure 7. In order to compute this bias and resolution, distributions of frac-  
 285 tional inverse momentum difference ( $\frac{p_{MCS}^{-1} - p_{Range}^{-1}}{p_{Range}^{-1}}$ ) in bins of range-based momentum  $p_{Range}$   
 286 are fit to gaussians and the mean of the fit determines the bias while the width of the fit determines  
 287 the resolution for that bin. Inverse momentum is used here because the binned distributions are  
 288 more gaussian (since the Highland formula measures inverse momentum in terms of track angles  
 289 that have reasonably Gaussian errors). Note that simply using the mean and RMS of the binned  
 290 distributions yields similar results. Also shown in this figure are the bias and resolutions for an anal-  
 291 ogous simulated sample consisting of full BNB simulation with CORSIKA-generated [19] cosmic  
 292 overlays passed through an identical reconstruction and event selection chain. Rather than hand

scanning this sample, true simulation information was used by requiring the longest reconstructed track matched well in terms of true starting and stopping point of the  $\nu_\mu$ CC muon. This removes any mis identifications or interference from the simulated cosmics.

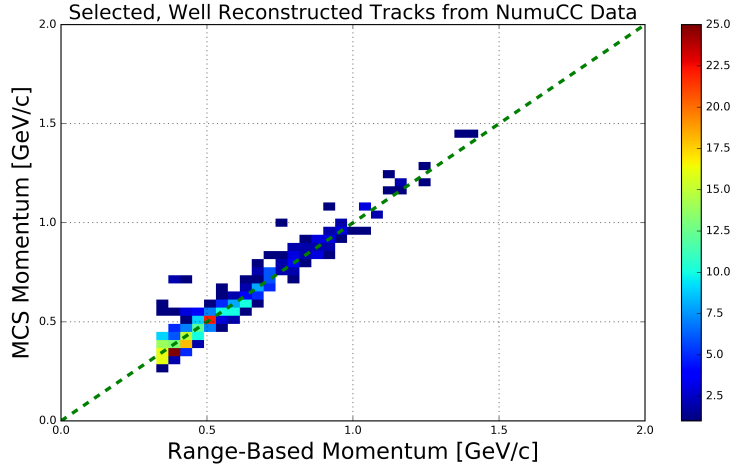


**Figure 6.** *MCS computed momentum versus range momentum for the automatically selected beam neutrino-induced fully contained muon sample in MicroBooNE data after hand scanning to remove poorly reconstructed tracks and obvious mis-identification (MID) topologies. The color ( $z$ ) scale indicates number of tracks.*

Figure 7 indicates a bias in the MCS momentum calculation on the order of a few percent, with a resolution that decreases from about 10% for contained reconstructed tracks in data and simulation with range momentum around 0.45 GeV/c (which corresponds to a length of about 1.5 meters) to below 5% for contained reconstructed tracks in data and simulation with range momentum about 1.15 GeV/c (which corresponds to a length of about 4.6 meters). Resolution improving with length of track is intuitive; the longer the track, the more angular scattering measurements can be made to improve the likelihood. In general the bias and resolutions agree between data and simulation within uncertainty.

304

### 305 5.5 Impact of Highland Formula Tuning

306 In order to examine the impact of the Highland formula tuning described in Section 2.1, the fractional  
 307 bias and resolution on the simulated sample of contained muons described in Section 5.4  
 308 both with the nominal Highland formula (Equation 2.2) and with the retuned Highland formula  
 309 (Equation 2.5) are shown in Figure 8. Tuning the Highland formula improves the magnitude of  
 310 the fractional bias to below 2%, and improves the fractional resolution by 2-3%, with the most  
 311 improvement in the lowest momentum bins.

## 312 6 MCS Performance on Exiting Muons in MicroBooNE Simulation

313 This section quantifies the MCS algorithm performance on a sample of exiting muon tracks in  
 314 simulated BNB  $\nu_\mu$ CC interactions within the MicroBooNE detector. The tracks are automatically

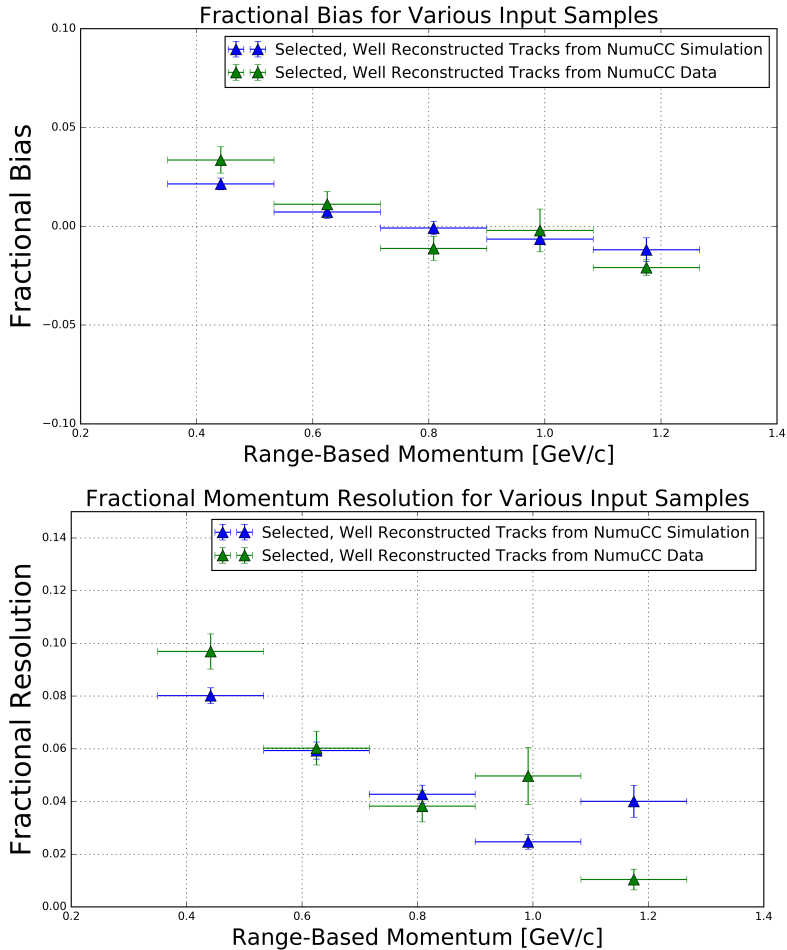


**Figure 7.** Inverse momentum difference (as defined in the text) fractional bias (top) and resolution (bottom) for automatically selected contained  $\nu_\mu$ CC-induced muons from full simulated BNB events with cosmic overlay where the track matches with the true muon track (blue), and automatically selected (see text) contained  $\nu_\mu$ CC-induced muons from MicroBooNE data (green).

reconstructed by the same “pandoraNuPMA” algorithm described in Section 3.1, and all tracks have at least one meter contained within the TPC. This simulation does not include space charge effects which are non-negligible near the TPC walls. The MCS momentum versus true momentum for this sample of 28,000 exiting muon tracks can be seen in Figure 9.

The distribution of  $(\frac{p_{MCS}^{-1} - p_{true}^{-1}}{p_{true}^{-1}})$  is shown for four representative bins of true momentum in Figure 10, along with the Gaussian fit to each. Low momentum tails in which the MCS momentum is an underestimation of the true momentum can be seen outside of the central gaussian fit. These tails can be attributed to reconstruction effects.

The algorithm fractional bias and resolution as a function of true momentum are shown in Figure 11. It can be seen that the bias is below 4% for all momenta, and the resolution is roughly 14% in the relevant momentum region for BNB  $\nu_\mu$ CC muons (below 2 GeV/c). The resolution worsens

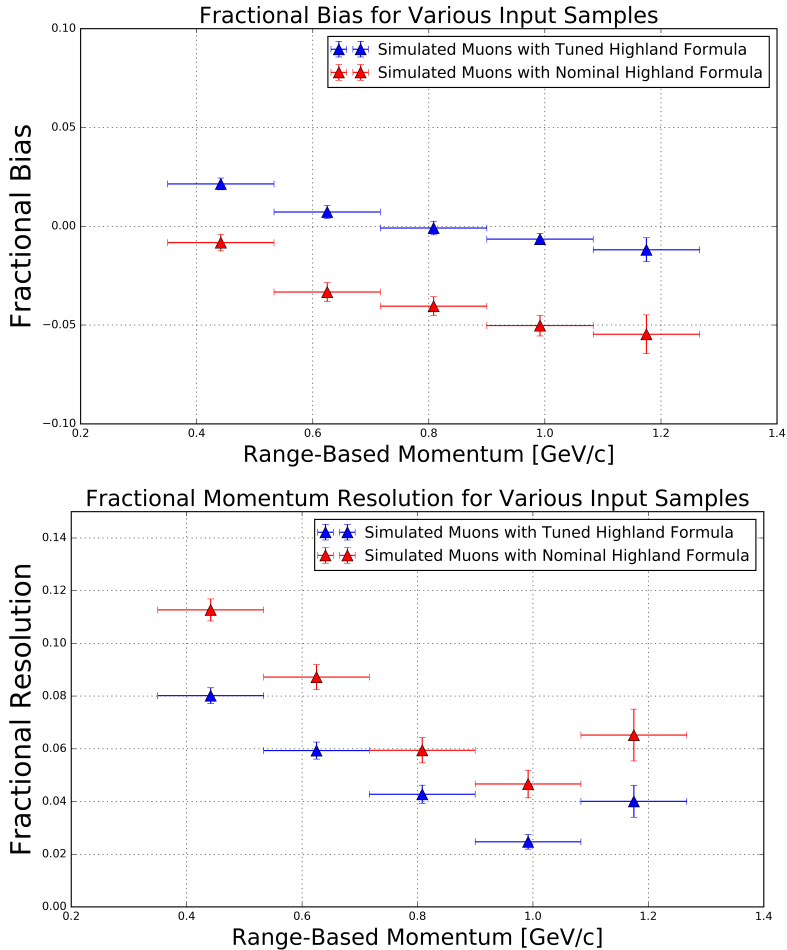


**Figure 8.** Inverse momentum difference (as defined in the text) fractional bias (top) and resolution (bottom) for automatically selected contained  $\nu_\mu CC$ -induced muons from full simulated BNB events with cosmic overlay where the track matches with the true muon track both using the nominal Highland formula (Equation 2.2) (red) and the retuned Highland formula (Equation 2.5) (blue).

for muon momenta above this region because the angular scatters begin to be comparable with the detector resolution term of 3 mrad. Note that the resolution improves for longer lengths of track contained, with 10% resolution for muons below 2 GeV/c with more than 3.5 meters contained.

331

## 332 7 Conclusions

333 We have described a multiple Coulomb scattering maximum likelihood method for estimating the  
 334 momentum of a three dimensional reconstructed track in a LArTPC and have provided motivation  
 335 for development of such a technique. Using MC, we have shown that the standard Highland formula  
 336 should be re-tuned specifically for scattering in liquid argon. After benchmarking range-based  
 337 momentum determination techniques with MicroBooNE MC, we have demonstrated the accuracy  
 338 and precision of the MCS-based momentum reconstruction in MicroBooNE data by comparing its

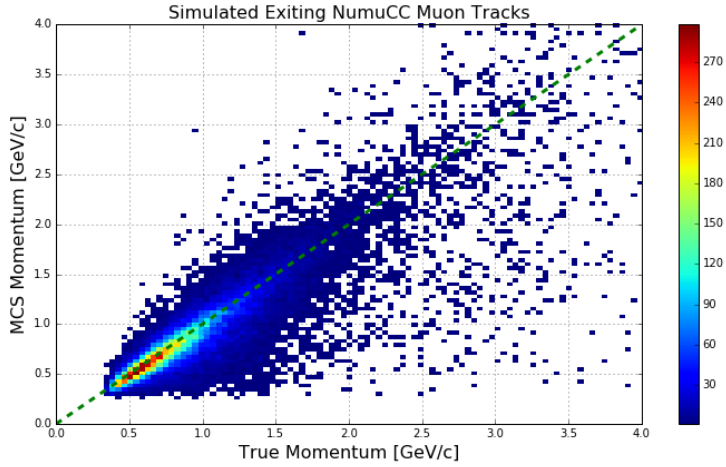


**Figure 9.** MCS computed momentum versus true momentum for the sample of simulated exiting BNB  $\nu_\mu$ CC muons in MicroBooNE with at least one meter of track contained within the TPC.

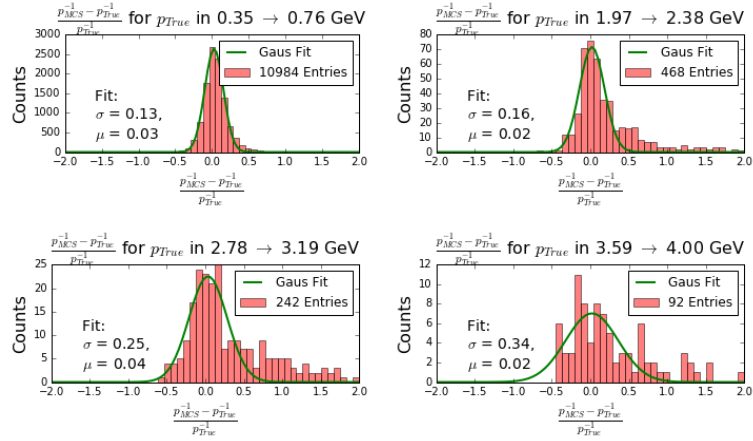


**Figure 10.** Fractional momentum difference for a few representative bins of true momentum.

339 performance to the range-based method. For 398 fully-contained BNB  $\nu_\mu$ CC-induced muons, the  
 340 MCS method exhibits a fractional bias below 3% and a momentum resolution below 10%, agreeing  
 341 with simulation predictions. Using MC simulation of uncontained muon tracks in MicroBooNE  
 342 with at least one meter contained, the MCS-based reconstruction is shown to produce a fractional  
 343 bias below 4% and a momentum resolution of better than 15% for muons in the relevant BNB  
 344 energy region of below 2 GeV.

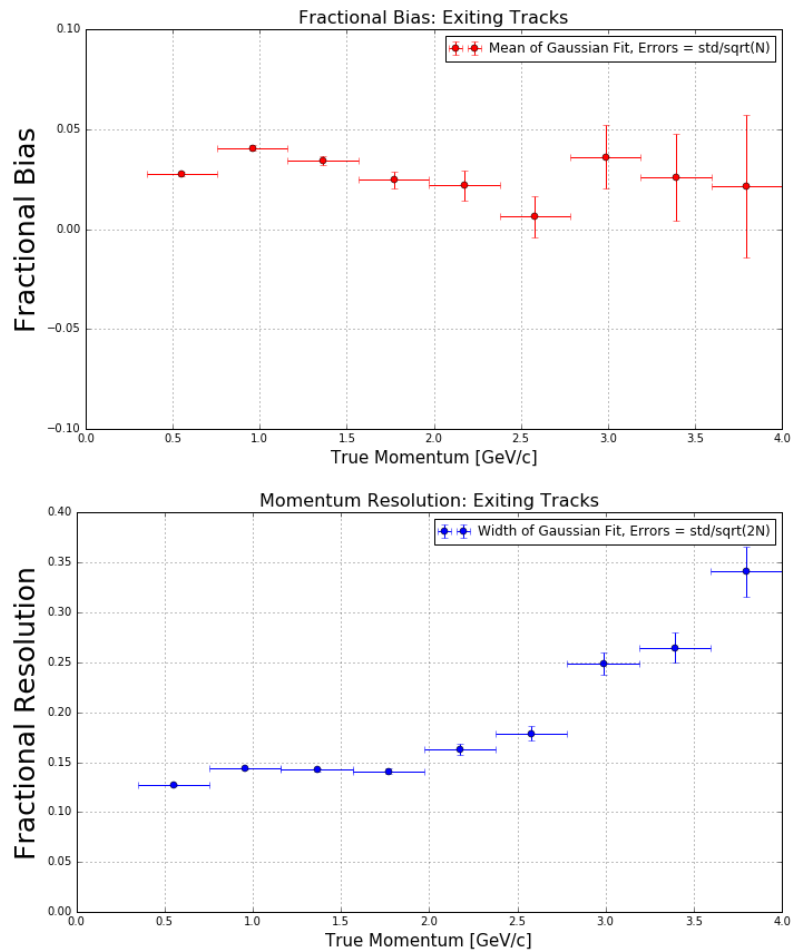


**Figure 11.** MCS momentum fractional bias (top) and resolution (bottom) as a function of true momentum from a sample of exiting reconstructed muon tracks.

345 **References**

- 346 [1] A. A. Aguilar-Arevalo *et al.* [MiniBooNE Collaboration], Improved Search for  $\bar{\nu}_\mu \rightarrow \bar{\nu}_e$  Oscillations  
347 in the MiniBooNE Experiment, Phys. Rev. Lett. **110**, 161801 (2013).  
348 doi:10.1103/PhysRevLett.110.161801 [arXiv:1207.4809 [hep-ex], arXiv:1303.2588 [hep-ex]].
- 349 [2] C. Adams *et al.* [LArTPC Collaboration], arXiv:1309.7987 [physics.ins-det].
- 350 [3] R. Acciarri *et al.* [MicroBooNE Collaboration], “Design and Construction of the MicroBooNE  
351 Detector,” arXiv:1612.05824 [physics.ins-det].
- 352 [4] R. Acciarri *et al.* [MicroBooNE Collaboration], “Study of Space Charge Effects in MicroBooNE”  
353 www-microboone.fnal.gov/publications/publicnotes/MICROBOONE-NOTE-1018-PUB.pdf.
- 354 [5] V. L. Highland, Some Practical Remarks on Multiple Scattering, Nucl. Instrum. Methods **129** (1975)  
355 104-120.
- 356 [6] K. Kodama *et al.* [DONUT Collaboration], Phys. Lett. B **504**, 218 (2001)  
357 doi:10.1016/S0370-2693(01)00307-0 [hep-ex/0012035].
- 358 [7] N. Agafonova *et al.* [OPERA Collaboration], New J. Phys. **14**, 013026 (2012)  
359 doi:10.1088/1367-2630/14/1/013026 [arXiv:1106.6211 [physics.ins-det]].
- 360 [8] G. Giacomelli [MACRO Collaboration], Braz. J. Phys. **33**, 211 (2003)  
361 doi:10.1590/S0103-97332003000200008 [hep-ex/0210006].
- 362 [9] A. Ankowski *et al.* [ICARUS Collaboration], “Measurement of through-going particle momentum by  
363 means of multiple scattering with the ICARUS T600 TPC,” Eur. Phys. J. C **48**, 667 (2006)  
364 doi:10.1140/epjc/s10052-006-0051-3 [hep-ex/0606006].
- 365 [10] M. Antonello *et al.*, “Muon momentum measurement in ICARUS-T600 LAr-TPC via multiple  
366 scattering in few-GeV range,” arXiv:1612.07715 [physics.ins-det].
- 367 [11] G. R. Lynch and O. I. Dahl, Nucl. Instrum. Methods Section B (Beam Interactions with Materials  
368 and Atoms) **B58**, **6** (1991).
- 369 [12] S. Agostinelli et al. Nucl. Instrum. Methods Phys. Res. **A506250-303** (2003)
- 370 [13] F. Cavanna *et al.* [LArIAT Collaboration], arXiv:1406.5560 [physics.ins-det].
- 371 [14] J. S. Marshall and M. A. Thomson, “The Pandora Software Development Kit for Pattern  
372 Recognition,” Eur. Phys. J. C **75**, no. 9, 439 (2015) doi:10.1140/epjc/s10052-015-3659-3  
373 [arXiv:1506.05348 [physics.data-an]].
- 374 [15] D. E. Groom, N. V. Mokhov and S. Striganov, “Muon Stopping Power and Range Tables: 10 MeV -  
375 100 TeV” Table 5, <http://pdg.lbl.gov/2012/AtomicNuclearProperties/adndt.pdf>
- 376 [16] H. Bichsel, D. E. Groom, S.R. Klein, “Passage of Particles Through Matter” PDG Chapter 27, Figure  
377 27.1 <http://pdg.lbl.gov/2005/reviews/passagerpp.pdf>
- 378 [17] Table 289: Muons in Liquid argon (Ar) [http://pdg.lbl.gov/2012/AtomicNuclearProperties/MUON\\_ELOSS\\_TABLES/muonloss\\_289.pdf](http://pdg.lbl.gov/2012/AtomicNuclearProperties/MUON_ELOSS_TABLES/muonloss_289.pdf)
- 380 [18] “Stopping Powers and Ranges for Protons and Alpha Particles,” ICRU Report No. 49 (1993); Tables  
381 and graphs of these data are available at <http://physics.nist.gov/PhysRefData/>
- 382 [19] D. Heck, J. Knapp, J. N. Capdevielle, G. Schatz, T. Throw, *CORSIKA: A Monte Carlo Code to*  
383 *Simulate Extensive Air Showers*, Forschungszentrum Karlsruhe Report FZKA 6019 (1998)